NUMERICAL ANALYSIS OF HEAT TRANSFER PERFORMANCE OF A FLAT-PLATE SOLAR COLLECTOR

Diogenes Linard Aquino Freitas,eng.diogeneslinard@gmail.com
Mikaele L. Diniz, mikaele.diniz@cear.ufpb.br
Gilberto Augusto Amado Moreira,gilberto@cear.ufpb.br
Zaqueu Ernesto da Silva, zaqueu@cear.ufpb.br
Centro de Energias Alternativas e Renováveis, Universidade Federal da Paraíba, Cidade Universitária - João Pessoa – PB, CEP 58051-900

Adriana Lessa Viana
Universidade Federal de Minas Gerais, Av. Antônio Carlos, 6627 - Pampulha - Belo Horizonte – MG, CEP 31270-901

Abstract. *Solar energy is becoming an alternative for the limited fossil fuel resources. One of the simplest and most direct applications of this energy is the conversion of solar radiation into heat, which can be used in water heating systems. A commonly used solar collector is the flat-plate. A lot of research has been conducted in order to analyze the flat-plate operation and improve its efficiency. This study presents a three-dimensional mathematical model for simulating the transient processes which occur in flat-plate liquid solar collectors. The differential equations were solved by the finite volume method in an iterative scheme using a CFD methodology for the commercial code ANSYS CFX. In order to evaluate the proposed method, an experiment was designed and conducted for several days under ambient conditions and flow rates. The comparison between the numerical and measured results of the transient fluid temperature at the collector outlet showed a satisfactory convergence. The proposed method is appropriate for the verification of the absorber and glass cover effectiveness, in addition to calculate the overall efficiency of the system along with the overall heat loss factor.*

Keywords*: Solar Energy, Flat Plate Solar Collector, Thermal performance, Computational fluid dynamics (CFD)*

1. INTRODUCTION

Energy demand has grown in recent years as the development and global population increase. Most of this energy is produced by fossil fuels such as oil and natural gas. Besides all the impacts on the environment for these fuels and CO2 released during combustion, these are not renewable energy sources. To avoid need of decrease energy consumption decrease is improbable , it is necessary to prioritize the use of renewable and clean energy sources.

An example of inexhaustible and clean energy is energy from the sun. The main component of any solar system is a solar collector. This is a device which absorbs solar radiation, converts it into heat, and transfers this heat to a fluid flowing through the collector. The solar energy thus collected is carried from the circulating fluid either directly to the hot water or space conditioning equipment or to a thermal energy storage tank from which can be drawn for use at night and/or cloudy days (Kabeel; Abdelgaied, 2014).

Solar collector has different application, such as; (i) a solar desalination unit, the solar collector is the main component of a solar desalination unit and any improvement in its efficiency will have a direct bearing on the water production rate and the product cost (Hallaj andSelman, 2002). (ii) Solar heating systems and solar thermal power plants, respectively (Elminir,2006). (iii)Air-conditioning systems, solar energy is used for space heating, hot water production and thermally driven air-conditioning systems including desiccant cooling systems. This air-conditioning technique would be an alternative to vapor compression systems (Jurinak et al., 1984).

The simulation of water heating systems by solar energy can be accomplished through many system configurations. The aim of this work and develop a numerical model to be as input to optimize the supplement of hot water required for an adsorption cooling system.

2. EXPERIMENTAL SETUP

In the present study, the computational fluid dynamics (CFD) was employed to study the performance of the collector on water heating mode. A series of experimental data are based on the variation of the flow mass, as a function of variation of temperature of outlet. The analytical model can properly predict the dynamic thermal performance of the solar collector by comparing experimental and simulated data was validated.

2.1 CFD simulation

In this section a 3-dimensional CFD simulation of flat-plate thermal solar collectors is investigated. Commercial CFD simulation code ANSYS CFX (version 12.1) is used to solve the conservation equations for mass, momentum and energy. Next, the physical model and the computational procedure are presented under the followings assumptions:

1. The working fluid (air and water) is incompressible for operating range of solar air heaters since variation in density is very less;
2. Negligible radiation heat transfer and other heat losses;
3. The wall, absorber plate, tubes and roughness material are homogeneous and isotropic;
4. The flow is steady, fully developed, turbulent and three dimensional;
5. No-slip boundary condition is assigned to the walls in contact with the fluid in the model;
6. The thermal conductivity of the wall, absorber plate and roughness material are independent of temperature.

2.1.1. Resource for computational analysis

The model of the fluid domain used for analysis is built using ANSYS DESIGN MODELER V12.1. Grid is generated in ANSYS ICEM CFD V12.1. Then meshed model is exported to ANSYS CFX V12.1 to be analyzed. An assembled desktop computer having the following configuration is used e Processor e Intel Core I5 3.20 GHz CPU, RAM e 32 GB (8GBX4), Hard Disk e 2 TB, Graphic Card e Nvidia GTX 750 Ti, Operatingsystem e Window 10 Ultimate 64-bit.

2.1.2. Solution domain

The 3-dimensional solution domain used by CFD analysis has been generated as shown in Fig. 2. This domain is a horizontal flat plate solar collector on the absorber plate at the underside of the top of the plate while other sides are considered as smooth surfaces.

An uniform heat flux on the top wall boundary is considered for computational analysis, with their values shown in Table 4, and the side wall and bottom are assumed to be in adiabatic condition. The flat plate collector has 6 heat pipes, each with an absorber area of 1,57 m² and a diameter of heat pipe of 12,7mm. Figure 1 is a schematic drawing of the flat solar collector and its main dimensions and the Table 1 shows your measurements in millimeters. The operating parameters employed in this computational investigation are listed in Table 2.

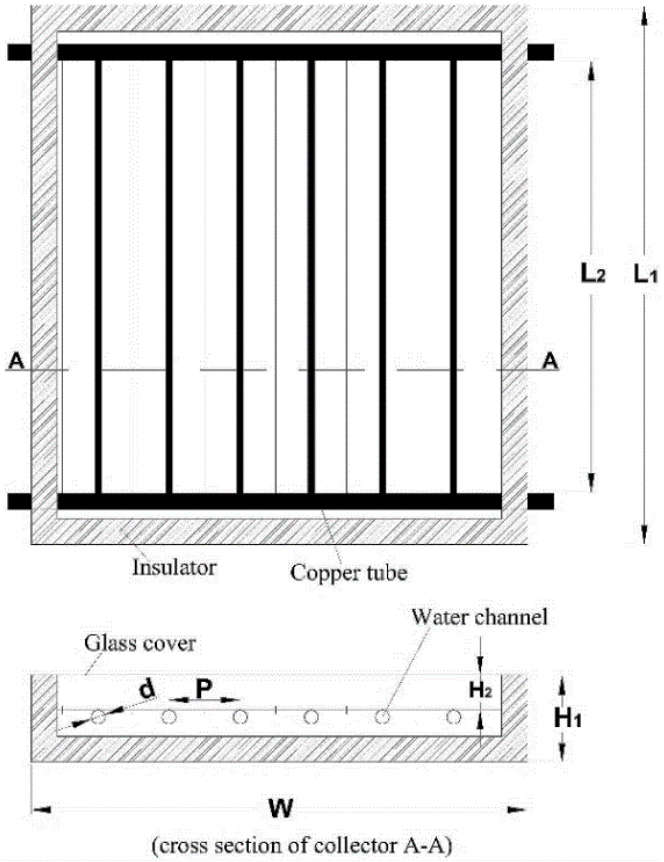

Figure 1. Layout of the solar collector

Table 1. Geometric parameters of the solar flat plate collector

L_1 (mm)	L_2 (mm)	W (mm)	H_1(mm)	H_2 (mm)	d (mm)	P (mm)
2080	1990	840	90	50	8	130

Table 2. Range of operation parameters for computational analysis

Operating parameters	Range
Uniform heat flux, (I)	1080 W/m²
Reynolds number, (R_e)	2000 – 6800 (5 values)
Prandtl number, (P_r)	5,20
Relative roughness of the pipe, (P/e)	1,0 e-5

2.1.3. Grid generation

A fine non-uniform mesh of the domain is done using ANSYS software, is used to resolve the laminar sub-layer, which is and shown in Fig. 2. The grids are generated so as to be very fine when the low Reynolds number turbulence models is used. Present non-uniform quadrilateral mesh containing approximately 32k elements with non-uniform quad grid of 0.2 mm cell size (minimum value). This size is suitable to resolve the laminar sublayer.

For grid independence test, the nodes numbers are varied from 2.3k to 7.4k in five steps. It is found that after 6.7k elements, further increase in cells has less than 1% variation in Nusselt number and friction factor value, which was taken as criterion for grid independence.

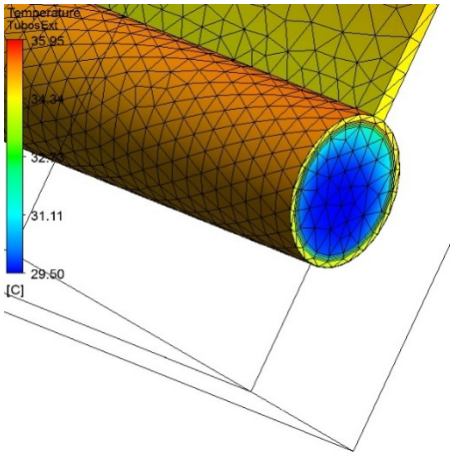

Figure 2. Computational domain and grid setup

2.1.4. Governing equation

The flow phenomenon in flat plate solar collectors is governed by the steady 3-dimensional form of the continuity, the time-independent incompressible Navier-Stokes equations and the energy equation. In the Cartesian tensor system these equations can be written as:

Continuity equation:

$$\frac{\partial}{\partial x_i}(\rho u_i) = 0 \qquad (1)$$

Momentum equation:

$$\frac{\partial}{\partial x_i}(\rho u_j u_j) = -\frac{\partial p}{\partial x_i} + \frac{\partial}{\partial x_j}\left[\mu\left(\frac{\partial u_i}{\partial x_j} + \frac{\partial u_j}{\partial x_i}\right)\right] + \frac{\partial}{\partial x_j}\left(-\rho\overline{u_1' u_j'}\right) \qquad (2)$$

Energy equation:

$$\frac{\partial}{\partial x_i}\left(\rho u_j T\right) = \frac{\partial}{\partial x_j}\left((\Gamma + \Gamma_t)\frac{\partial T}{\partial x_j}\right) \qquad (3)$$

where Γ and Γ t are molecular thermal diffusivity and turbulent thermal diffusivity, respectively, and are given by:
$\Gamma = {}^{\mu}/_{\mathrm{P_r}}$ and $\Gamma_t = {}^{\mu_t}/_{\mathrm{P_{r_t}}}$

The Eqs. (1) and (2) are also called the Reynolds-averaged Naviere Stokes equations. Additional terms $-\rho\overline{u_1' u_j'}$now appear in Eq. (2) that represents the effects of turbulence. These Reynolds stresses, $-\rho\overline{u_1' u_j'}$must be modeled in order to close Eq. (2). The Reynoldsaveraged approach to turbulence modeling requires that the Reynolds stresses in Eq. (2) are appropriately modeled. A common method employs the Boussinesq hypothesis to relate the Reynolds stresses to the mean velocity gradients:

$$-\rho\overline{u_1' u_j'} = \mu_t\left(\frac{\partial u_i}{\partial x_j} + \frac{\partial u_j}{\partial x_i}\right) \qquad (4)$$

The Boussinesq hypothesis is used in the k-ε models (Standard k-ε model, Renormalization-group k-ε model, Realizable k-ε model), and the k-ω models (Standard k-ω and Shear stress transport k-u model). The advantage of this approach is the relatively low computational cost associated with the computation of the turbulent viscosity,μt (ANSYS, 2003).

The turbulence model k-ε (Launder and Spalding, 1974) models the characteristics scales of turbulent viscosity through the turbulent kinetic energy (k) and the turbulent dissipation (ε). The RNGKE model (Yakhot and Orzag, 1994) is an improvement of the previous model, based on the renormalization group of the Navier-Stokes equations. The transport equations for generating turbulence and dissipation are the same k-ε model, the only difference is in the constants. In CFX 11.0 (ANSYS, 2007) the model uses a scalable RNGKE logarithmic function on the walls, this model limits the lowest value of the wall dimensionless distance used in the calculation of variables.

The SST model (Wilcox, 1994) involves a combination of turbulence models k-ω (Speziale, 1991) near the surface, which is based on the k relationship with the dissipation rate specifies the turbulence (ω), and k-ε (Launder and Spalding, 1974) core flow. The model includes a function that changes the turbulent viscosity to consider the transport of turbulent shear stresses. In CFX 11.0 (ANSYS, 2007) the SST model uses an automatic treatment for the wall function that changes the logarithmic region to the viscous sub-layer according to refining the mesh near the wall.

2.1.5. Boundary condition

The solution domain of the considered 3D, flow is geometrically complex. It is a rectangle on the XY plane, enclosed by the inlet, outlet and wall boundaries. The working fluid in all cases is water. Assuming to remain constant at average bulk temperature, the thermo-physical properties of working fluid and absorber plate are illustrated in Table 3.

Table 3. Thermo-physical properties of working fluid (water) and absorber plate (copper) for computational analysis.

Properties	Working fluid (water)	Absorber plate (copper)
Specific heat, (C_p) [KJ kg^{-1} K^{-1}]	4,18	0,385
Density, (ρ) [kg m^3]	1000	8933
Viscosity, (μ) [N s m^{-2}]	760 e-03	-
Thermal conductivity, (k) [W m^{-1} K^{-1}]	620	401

2.2. Experimental Model

This work aims to optimize and simulate an active system of water heating on a Flat Plate Solar Collectors, and evaluate its efficiency. As experimental apparatus for this work, we make use of one water pump with a capacity of 10 L/min, a solar collector with glass cover, a cooling unit (cooling capacity of 2850 Btu / hr), ball valve, a structure of metal to modify the slope of the flat plate, and sensors for acquisition of the main variables, as shown in Fig.3-a.

This mechanism allows us to vary the plate slope, the working fluid inlet temperature (keeping constant) and the mass flow, providing a different operating condition, and calculates the thermal efficiency in each collector.

2.2.1 Experimental Setup

The sensors are installed near the solar panel, as shown in Fig.3-b. To measure the solar radiation, we use was done using two pyranometer, one inclined for measuring solar radiation(sensitivity 8,18x10-6 V / Wm^{-2}) located in the same plane than collector and another for measuring the total radiation plane (8,92x10 -6 V / Wm^{-2}), near of direction and wind speed sensors, on the metal structure. Direction and speed sensors are potentiometers W200P windvane and anemometer A100LK / A100LM. The velocity sensor measures rates 0.15 m / s to 75 m / s. To measure temperature, it was used two NTC SB59sensors operating at temperatures from -50 to 200° C, one sensor was located fluid inlet and the other at the outlet. To read these temperatures the analog voltage signal was amplified in a gain of 101 V/V.

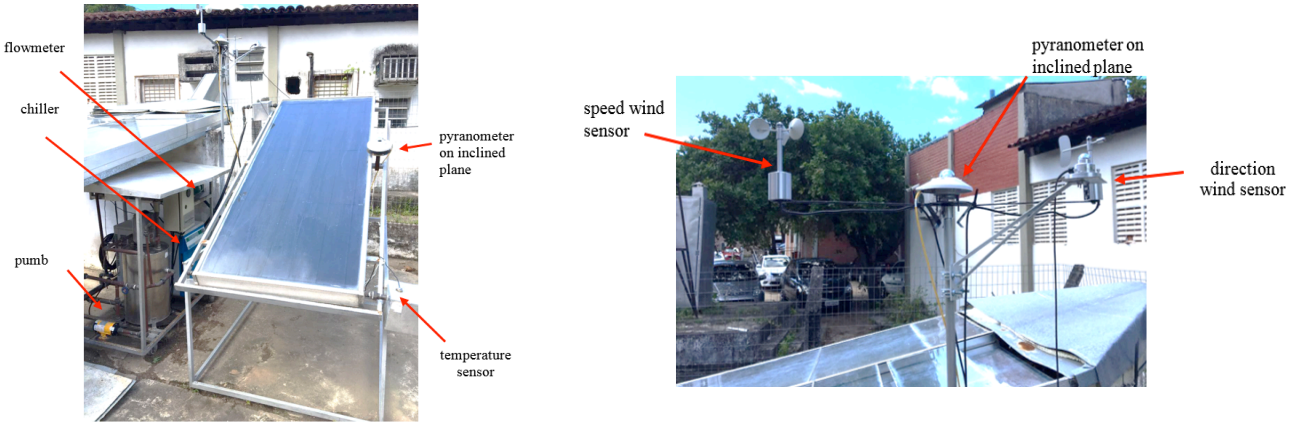

(a) *(b)*

Figure 3. (a) Experimental apparatus of the solar heating system, and (b) metal frame with positioning sensors.

The main performance parameter of a solar thermal panel is the collector efficiency, which is defined as the ratio of the collected thermal power over the total incident solar power. Instantaneous efficiency curve is the main criterion for the thermal performance of a flat plate solar collector, which can be calculated by the following equation in Eq. (5).

$$\eta = \frac{\dot{Q}_u}{A_c I_t} = F_R(\tau\alpha) - F_R U_L \frac{(T_f - T_a)}{I_T} \tag{5}$$

where F_R is the heat removal factor; U_L is the heat loss coefficient; $(\tau\alpha)$ is the collector effective transmittance–absorptance product, which can be measured by the experiment. Eq. (5) indicates that η can be represented by a linear relation with the parameters $(T_f - T_a)/I_T$. The term of $F_R(\tau\alpha)$ represents the intercept of the efficiency line with the y-axis, which is the maximal efficiency for the solar collector.

In the practical applications, solar collectors usually work under dynamic weather conditions. So the thermal performances of the solar collectors are dynamic and the steady-state model derived from steady-state test (SST) method in ANSI/ASHRAE (2003) does not pertain to the dynamic conditions. The acquisition of the data were monitored in real time by a graphical interface developed in LabVIEW™, according to Fig.4, and from Eq.(5), which is generally known by the steady-state test (SST) method, curves were raised the thermal efficiency as a function of the ratio between the water inlet temperature difference and the environment with the incident solar radiation, and then compared with the results of numerical simulation model adopted. On the other hand, the product $F_R U_L$ of this equation represents the slope of the efficiency line, and its absolute value reflects the total heat loss factor for the solar collector.

The main limitation of this model is that it can not reproduce the spatial temperature profile inside the collector, therefore it causes errors in heat losses calculation and, consequently, in the outlet water temperature result. Beyond that, analyzing the influence of the thermal capacitance on the long term behavior of the solar collector, Wijeysundera (1978) showed that the steady state approach gives good results in predicting the daily energy collection only when hourly averaged meteorological data is used. If the radiation intensity changes quickly, the dynamic effects become most pronounced and the steady state model overestimates the useful energy collection. In these conditions transient approaches provide better results. The author concluded that the main usefulness of the dynamic approach in modeling the solar collector is detected in the short term study and in predicting the outlet temperature behavior as a consequence of the fluctuations of the climatic data.

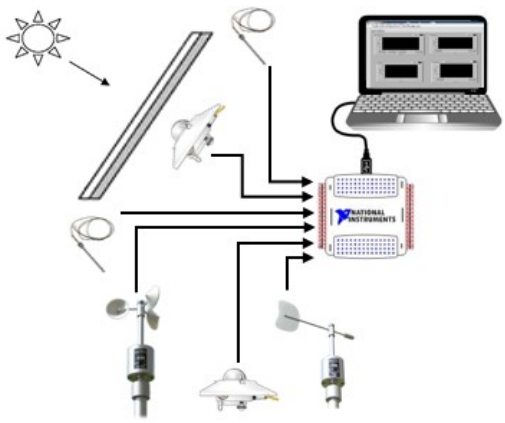

Figure 4.Flowchart data acquisition

3. COMPARISON OF RESULTS

Experimental data of the efficiencies for five different mass flow rates (1,0 at 3,0 L/min) has been recorded under the condition of 16° tilt of solar collector. A minimum of 20 data points at five different flow rate (fluid temperatures) were obtained using SST method to determine the thermal efficiency curve ηvs $(T_f - T_a)/I$of the SAC. Table 4 lists the corresponding measured data for model validation, i.e. the average outdoor temperature, the solar radiation, the average inlet water temperature and heat flux, within the time.

Table 4. Results of measured mean values for model validation

Case	Time and Hour	T_{in} [°C]	T_{out} [°C]	T_a [°C]	Mass flow [Kg/s]	Heat flux [W]	Irradiation inclined [W/m²]	Irradiation flat [W/m²]
1	05/13/2016 10:45h -10:50h	34	48	34	0,011 (1 L/min)	607,81	1101,81	910,22
2	05/13/2016 11:20h -11:25h	35	45	35	0,016 (1,5 L/min)	616,47	1088,92	891,22
3	04/28/2016 10:37h-10:41h	29	37	33	0,021 (2 L/min)	733,25	1122,63	947,63
4	04/30/2016 10:45h-10:50h	30	35	33	0,026 (2,5 L/min)	543,58	1165,59	985,88
5	04/30/2016 14:30h-14:35h	29	32	34	0,032 (3 L/min)	360,99	943,83	752,92

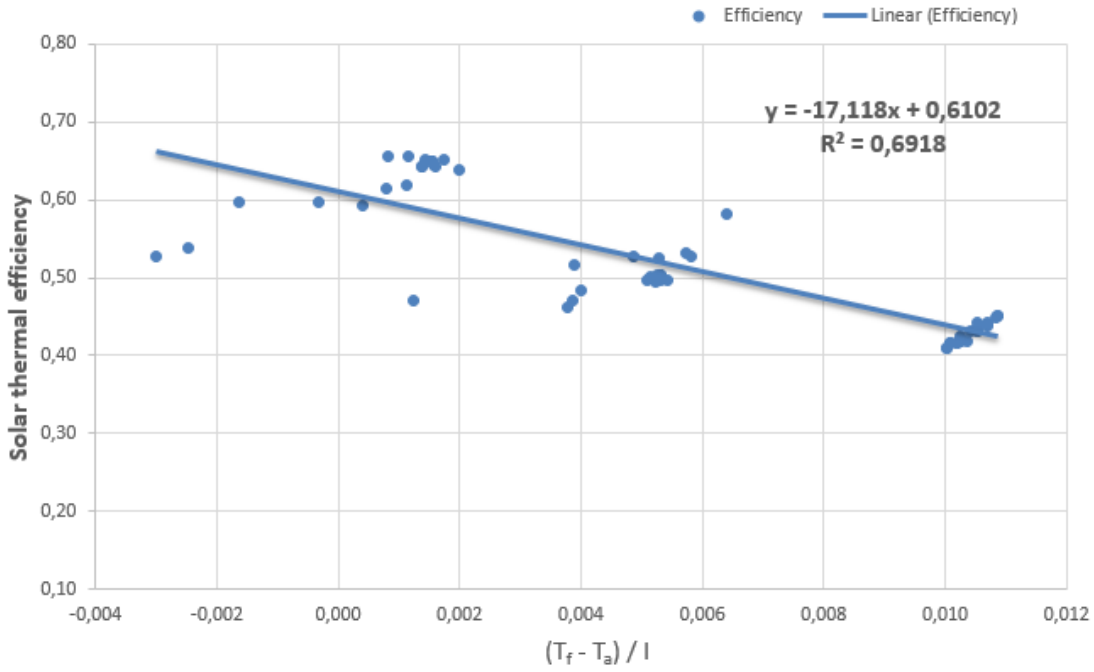

Figure 5.Relationηversus $(T_f - T_a)/I$ for solar collector.

Figure 5 represents the instantaneous efficiency curve of the designed flat plate solar collector with a vertical solar radiation on the solar collector, 16° tilt of the solar collector and a 50 mm air gap distance. The collection efficiency increases with the increase of inlet water mass flow rate, and then tends to stay invariant with other variables keeping constant. In this paper, the best inlet water mass flow rate for this flat plate solar collector is 3,0 L/min. The regression line for the flat plate collector was found as: $\eta = 0{,}6102 - 17{,}118\left(\frac{T_f - T_a}{I}\right)$ with a correlation coefficient of 0,6918. Therefore, the maximal efficiency of this solar collector is 0,6102 and the total heat loss factor is 17,118.

The CFD simulation result was validated using experimental data described above. Table 5 lists the comparison of the outlet water temperature between the numerical results and the experimental ones. Reasonable agreement was found between these two sets of results, giving the maximum relative error of 4,53% for the outlet water temperature.

Table 5. Results of predicted water temperature compared with experimental data

Case	CDF outlet water temperature (°C)	Experimental outlet water temperature (°C)	Relative error (%)
1	47,25	49,09	3,75
2	44,21	46,31	4,53
3	37,41	38,89	3,81
4	35,02	34,37	1,89
5	33,17	32,12	3,27

The results ilustrated in Fig.6 shows the temperature distribution in specific regions of the computational domain's, which can be observe as the ability to play concentration local heat that can be optimized. One of the suggestions for further work is play back the model to produce more energy efficient equipment and thereby minimize power consumption in devices that need heated fluid. One application of this research is the ability of solar collectors to supply heated water to a cooling unit by adsorption existing in the laboratory.

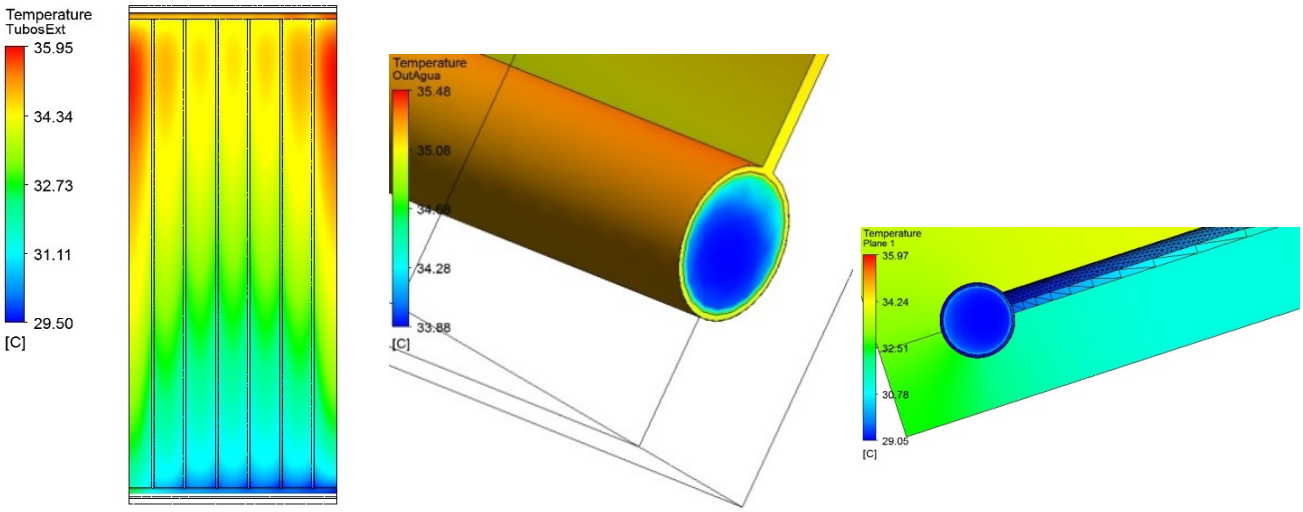

(a) (b) (c)

Figure 6.Numerical results of the temperature field on the plate (a) in detail at the input (b) and a side view (c).

4. CONCLUSION

The most experimental value of the solar collector efficiency was in the case of conditions 5. The points of the relationship ηversus $(T_f - T_a)/I$of solar collector, showed a good approximation to the literature, where the average temperature of the fluid increases, along with a decrease in efficiency. Increasing the water mass flow results in decrease in the outlet water temperature and increase in the collector's thermal efficiency. However, the collector has a high coefficient of overall heat loss.

The values of the measured radiation do not behave constant, which caused a large standard deviation in the points of efficiency.

In the mesh sensitivity study noted that although significantly influence the results, the inflation mesh parameters influence the bit mesh size in the order of thousands of elements. The parameters of the surface control loop also influence significantly the results, but have a large increase in the number of elements and nodes of the mesh, in the order of millions.

It has been observed that the turbulence models that use a next formulation wall based on ω, ie Standard k-ω and Shear stress transport k-u model, show a well organized and less intense convection compared with calculated by the model based on ε near the wall, ie RNGKE and k-ε.

It was shown in this study that the methodology proposed using the commercial code ANSYS CFX 12.1®, with the SST turbulence model and suitable mesh is able to simulate the engineering purposes.

5. ACKNOWLEDGMENTS

The authors would like to thank the National Council for Scientific and Technological Development (CNPq), projects nº 460258/2014-1.

6. REFERENCES

ANSI/ASHRAE Standard 93-2003. Methods of testing to determine the thermal performance of solar collectors. Atlanta: ASHRAE Inc.; 2003.

ANSYS CFX 11.0, User manual, ANSYS Europe Ltd., 2007.

ANSYS CFX. 12.1. Documentation. ANSYS, Inc; 2003-04

H.K. Elminir, "Optimum solar flat-plate collector slope: case study for Helwan, Egypt", Energy Conversion and Management 47 (2006) 624–637.

Jurinak, J.J., Mitchell, J.W., Beckman, and W.A., "Open-cycle desiccant air conditioning as an alternative to vapor compression cooling in residential applications". Journal of Solar Energy Engineering, (1984) 106, 252–260.

KABEEL, A. E.; ABDELGAIED, M. An innovative solar water collector using heat pipe with inner rings. IREC 2014 - 5th International Renewable Energy Congress, 2014.

Launder, B. E. and Spalding, D. B., The numerical computation of turbulent flow, Computer Methods in Applied Mechanics and Energy, vol. 3, 269-289, 1974.

Menter, F. R., Two-equation eddy-viscosity turbulence models for engineering applications, AIAA-Journal, vol. 32, 269-289, 1994.

S. Al Hallaj and J. R. Selman, "A comprehensive study of solar desalination with humidification–dehumidification cycle", MEDRC Series of R&D Reports. Project No. 98-BS-032b; (2002).

Speziale, C. G, Sparkar, S, Gatski, T. B., Modeling the pressure-strain correlation of turbulence: an invariant dynamical system approach, J. Fluid Mechanics, vol. 277, 245-272, 1991.

Wijeysundera, N.E. “Comparison of transient heat transfer models for flat plate collectors”. Sol Energy 1978; 21(6):517–21.

Wilcox, D. C., Turbulence modeling for CFD, DCW Industries Inc., La Cañada, Estados Unidos da America, 1994.

Yakhot, V., Orzag, S., Renormalization group analysis of turbulence, J. of Sci. Comput., vol. 1, 1-51, 1986.

7. RESPONSIBILITY NOTICE

The following text, properly adapted to the number of authors, must be included in the last section of the paper:The authors is are the only responsible for the printed material included in this paper.